Photoinduced Fluorescence Enhancement in Mono- and Multilayer Films of CdSe/ZnS Quantum Dots: Dependence on Intensity and Wavelength of Excitation Light

Takafumi Uematsu,* Shinya Maenosono, and Yukio Yamaguchi

Department of Chemical System Engineering, School of Engineering, The University of Tokyo, Hongo 7-3-1, Bunkyo-ku, Tokyo 113-8656, Japan

Received: January 19, 2005; In Final Form: March 2, 2005

Photoinduced fluorescence enhancement (PFE) behavior in mono- and multilayer films of CdSe/ZnS core/shell quantum dots (QDs) on glass substrates was investigated using various intensities and wavelengths of excitation light. CdSe/ZnS QDs capped with tri-*n*-octylphosphine oxide (TOPO) were produced using colloidal chemical synthesis, and mono- and multilayer QD films were fabricated on glass substrates by spin coating. The fluorescence quantum yield (QY) of the QD monolayer was greatly enhanced by continuous irradiation in a dry nitrogen atmosphere, whereas the QD multilayer showed a small enhancement of the QY or fluorescence intensity decay. In addition, the shorter the excitation wavelength, the more pronounced the PFE. The rate of increase of the QY increased with decreasing excitation intensities at any wavelength. These dependences were observed in both mono- and multilayer films. Our results suggest that the photoejection of electrons to the substrate is the origin of PFE. Assuming the charging effect of electrons trapped in the substrate, a phenomenological model is proposed to explain all of the experimental results, that is, the dependence on the intensity and wavelength of excitation light and the qualitative difference in PFE behavior between mono- and multilayer films.

1. Introduction

Colloidal semiconductor quantum dots (QDs) are attractive materials because of their size-dependent photophysical properties. In particular, various investigations into optical properties of single QDs, such as fluorescence intermittency,[1−5] spectral diffusion,[3,4] and photoionization,[6,7] have been performed using single-molecule and time-resolved spectroscopy. However, interdot interactions in QD ensembles have received little attention, except for Förster energy transfer.[8,9] One of the interesting properties of ensembles of CdSe QDs—reversible photoinduced fluorescence enhancement (PFE)—has been investigated under differing conditions.[10−20] However, the mechanism has not been clarified yet because the optical properties of CdSe QDs are very sensitive to the surrounding atmosphere[10−13] and capping agents.[11] In previous studies, the following four models have been proposed as mechanisms for the PFE phenomenon: (1) passivation of surface states on QDs by photoadsorbed gaseous molecules such as H_2O (photoactivation),[10−12] (2) photoinduced surface transformation[14] and/or photoinduced rearrangement of capping agents on QD surfaces[11,15] (phototransformation), (3) photoneutralization of local charged centers inside and outside QDs (photoneutralization),[16] and (4) photoionization of QDs and the ejected electrons, producing suppression of the ionization probability of the remaining neutral QDs (photoelectrification).[17−20]

To eliminate the effect of photoactivation, we have studied the PFE in a CdSe/ZnS QD film with a SiO_x protective layer[19] or under a dry N_2 atmosphere.[20] When a CdSe/ZnS QD submonolayer with a SiO_x protective layer was irradiated, the rate of increase of the fluorescence intensity increased with increasing packing density of QDs, and the maximum rate increase was observed in a trilayer QD film.[19] However, when a QD film was alternately irradiated by weak and strong excitation intensities in a dry N_2 atmosphere, the rate of increase of the fluorescence intensity changed reversibly.[20] The results could be qualitatively explained by the photoelectrification model, but they could not be explained by the phototransformation or photoneutralization models.[19,20] However, PFE in QD multilayers has not been studied in detail, and the influence of the substrate on PFE has not been clarified.

Here, we report the dependence of PFE behavior in mono- and multilayer films of CdSe/ZnS core/shell QDs on the intensity and wavelength of excitation light to investigate the role of the substrate. The two kinds of films were irradiated with light of various excitation intensities and wavelengths, and the experimental results are discussed on the basis of a photoelectrification model.

2. Model

2.1. Monolayer Model. Here we propose a model for PFE in a QD monolayer based on the model presented by Maenosono.[18] The following processes are considered to be relaxation pathways of bound excitons: band-edge radiative relaxation, radiative relaxation via surface states, nonradiative recombination, fast ionization−neutralization, and slow ionization processes. The fast ionization−neutralization process is expected to be a cause of fluorescence intermittency.[4,5] The rates of radiative relaxation and fast ionization have been reported to be on the order of 10^7 and 10^5-10^8 s^{-1}, respectively.[2,5] Comparing these processes, the slow ionization is a rather slow process and would cause a persistent darkening of QDs. Though it is not clear whether the trap sites exist in capping agents or in the substrate, Cherniavskaya et al. have reported that a substrate influences the slow photoionization behavior in the case of CdSe/CdS QDs on a silicon substrate with a thin SiO_2

* Corresponding author. E-mail: taka@chemsys.t.u-tokyo.ac.jp.

10.1021/jp050328k CCC: $30.25
Published on Web 04/13/2005

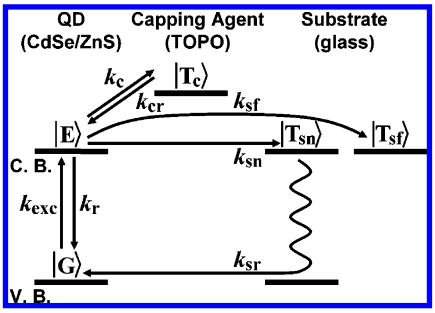

Figure 1. Schematic illustration of the electron transition processes among the five states of carriers.

layer.[7] Therefore, we consider that far (or deep) trap sites (T_{sf}) that are responsible for the slow ionization would exist in the substrate. However, near (or shallow) trap sites that are responsible for the fast ionization are expected to exist in both capping agents and the substrate (T_c and T_{sn}). In other words, we assume the following five states of carriers (Figure 1): ground state $|G\rangle$, excited state $|E\rangle$, trapped state in the capping agents $|T_c\rangle$, trapped state in the near trap sites in the substrate that is responsible for the fast ionization−neutralization process $|T_{sn}\rangle$, and trapped state in the far trap sites in the substrate that is responsible for the slow ionization $|T_{sf}\rangle$. The fractions of electrons situated in each state are expressed as ϕ_g, ϕ_e, ϕ_c, ϕ_{sn}, and ϕ_{sf}.

It has been reported that trap sites with various energy levels exist because fluorescence intermittency exhibits power-law statistics.[4,5] For simplicity, however, we assume a single rate constant for all pathways, neglecting the rate distribution (Figure 1): k_c (s^{-1}) for the $|E\rangle \rightarrow |T_c\rangle$ transition, k_{sn} (s^{-1}) for the $|E\rangle \rightarrow |T_{sn}\rangle$ transition, k_{sf} (s^{-1}) for the $|E\rangle \rightarrow |T_{sf}\rangle$ transition, k_{cr} (s^{-1}) for the $|T_c\rangle \rightarrow |E\rangle$ transition, and k_{sr} (s^{-1}) for the $|T_{sn}\rangle \rightarrow |G\rangle$ transition. The electron in T_{sn} is considered to return to $|G\rangle$ with k_{sr} (s^{-1}) via thermal relaxation through trap sites with various energy levels existing in the substrate. (For more details, see the Results and Discussion section.) The neutralization of electrons situated in $|T_{sf}\rangle$ is not considered because the rate of neutralization is thought to be much slower than those of other processes. On the basis of these assumptions, the rate equations for ϕ_c, ϕ_{sn}, and ϕ_{sf} can be written as

$$\frac{d\phi_c}{dt} = k_c\phi_e - k_{cr}\phi_c \tag{1}$$

$$\frac{d\phi_{sn}}{dt} = k_{sn}\phi_e - k_{sr}\phi_{sn} \tag{2}$$

$$\frac{d\phi_{sf}}{dt} = k_{sf}\phi_e \tag{3}$$

where t (s) is the irradiation time. The band-edge relaxation with recombination via surface states is classified as a radiative recombination process. Intrinsic nonradiative recombination is ignored because its rate is expected to be constant and does not affect the change in the fluorescence intensity of QDs. Thus, neglecting the Auger effects, the rate equations for ϕ_g and ϕ_e can be written as

$$\frac{d\phi_g}{dt} = -k_{exc}\phi_g + k_r\phi_e + k_{sr}\phi_{sn} \tag{4}$$

$$\frac{d\phi_e}{dt} = k_{exc}\phi_g - (k_r + k_c + k_{sn} + k_{sf})\phi_e + k_{cr}\phi_c \tag{5}$$

where $k_{exc} = \sigma I/(h\nu)$ (s^{-1}) and k_r (s^{-1}) are the rates of excitation and radiative recombination, respectively. Here, σ (cm^2), I (W/cm^2), h (J·s), and ν (cm^{-1}) are the absorption cross section of QDs, the excitation intensity, Planck's constant, and the frequency of the excitation light, respectively. Considering that k_{sf} is much smaller than the other rate constants, steady-state approximations are applied to eqs 1, 2, and 4. When $k_{sf} \ll k_{sn}$, one obtains $\overline{\phi_c} = (k_c/k_{cr})\overline{\phi_e}$, $\overline{\phi_{sn}} = (k_{sn}/k_{sr})\overline{\phi_e}$, and $\overline{\phi_g} = [(k_r + k_{sn})/k_{exc}]\overline{\phi_e}$. Here, $\overline{\phi_g}$, $\overline{\phi_e}$, $\overline{\phi_c}$, and $\overline{\phi_{sn}}$ represent the steady-state fractions of electrons situated in $|G\rangle$, $|E\rangle$, $|T_c\rangle$, and $|T_{sn}\rangle$, respectively. Combining these relations with the constrained condition $\overline{\phi_g} + \overline{\phi_e} + \overline{\phi_c} + \overline{\phi_{sn}} + \phi_{sf} = 1$, one obtains

$$\overline{\phi_e} = \frac{1 - \phi_{sf}}{\frac{k_r + k_{sn}}{k_{exc}} + 1 + \frac{k_c}{k_{cr}} + \frac{k_{sn}}{k_{sr}}} \tag{6}$$

It is assumed that a long-lived trapped electron situated in $|T_{sf}\rangle$ suppresses the further ionization of adjacent QDs because of the electrostatic blockade effect as discussed in ref 18. However, the electron in T_c is assumed to be free from the electrostatic effect because T_c is thought to be far enough from the substrate. Hence, k_{sn} and k_{sf} can be expressed as[18]

$$k_{sn} = k_{sn}^0(1 - \alpha\phi_{sf}) \tag{7a}$$

$$k_{sf} = k_{sf}^0(1 - \alpha\phi_{sf}) \tag{7b}$$

where k_{sn}^0 (s^{-1}) and k_{sf}^0 (s^{-1}) are the initial values of the fast ($|E\rangle \rightarrow |T_{sn}\rangle$) and slow ($|E\rangle \rightarrow |T_{sf}\rangle$) ionization rates, respectively. α is the blocking factor that represents the number of QDs whose ionization is suppressed by electrons situated in $|T_{sf}\rangle$.[18] By substituting eqs 7a and 7b into eqs 3 and 6, one obtains

$$\frac{d\phi_{sf}}{dt} = (1 - \alpha\phi_{sf})k_{sf}^0\overline{\phi_e} \tag{8}$$

$$\overline{\phi_e} = \frac{1 - \phi_{sf}}{\frac{k_r + k_{sn}^0(1 - \alpha\phi_{sf})}{k_{exc}} + 1 + \frac{k_c}{k_{cr}} + \frac{k_{sn}^0(1 - \alpha\phi_{sf})}{k_{sr}}} \tag{9}$$

The quantum yield (QY) of the QD monolayer, η_{mono}, that is defined as the number of emitted photons divided by the number of absorbed photons is written as

$$\eta_{mono} = C\frac{k_r\overline{\phi_e}}{k_{exc}} \tag{10}$$

where C is a constant of proportion between the true fluorescence intensity and the actual brightness of the fluorescence image that is obtained by confocal laser scanning microscopy (Experimental Section). Substituting the initial condition $\phi_{sf}|_{t=0} = 0$ into eq 9, the initial QY, $\eta_{0,mono}$, is given by eq 10 and written as

$$\eta_{0,mono} = \frac{Ck_r}{(1 + \beta + \gamma)k_{exc} + k_r + k_{sn}^0} \tag{11}$$

where $\beta = k_c/k_{cr}$ and $\gamma = k_{sn}^0/k_{sr}$. The value of ϕ_{sf} monotonically increases with irradiation time and saturates to $\phi_{sf} = \alpha^{-1}$

at $t = \infty$ as can be expected from eq 8. Thus, the saturated QY, $\eta_{s,mono}$, is written as

$$\eta_{s,mono} = \frac{Ck_r(1 - \alpha^{-1})}{(1 + \beta)k_{exc} + k_r} \quad (12)$$

2.2. Multilayer Model. In the case of QDs that do not contact the substrate, electron ejections to T_{sn} and T_{sf} can be neglected. Therefore, k_{sn}, k_{sf}, k_{sr}, ϕ_{sn}, and ϕ_{sf} can be considered to be be equal to 0, and eqs 1, 4, and 5 can be rewritten as

$$\frac{d\phi_c}{dt} = k_c\phi_e - k_{cr}\phi_c \quad (13)$$

$$\frac{d\phi_g}{dt} = -k_{exc}\phi_g + k_r\phi_e \quad (14)$$

$$\frac{d\phi_e}{dt} = k_{exc}\phi_g - (k_r + k_c)\phi_e + k_{cr}\phi_c \quad (15)$$

By applying steady-state approximations to eqs 13−15, one obtains

$$\overline{\phi_e} = \frac{1}{\frac{k_r}{k_{exc}} + 1 + \beta} \quad (16)$$

Hence, the QY of the QD layer that does not contact the substrate, η_{off}, is given by

$$\eta_{off} = \frac{Ck_r}{(1 + \beta)k_{exc} + k_r} \quad (17)$$

Assuming that the QY of the first layer near the substrate is the same as η_{mono} and that the QY of the upper layers is equal to η_{off}, the QY of the QD multilayer, η_{multi}, is given by

$$\eta_{multi} = \frac{\eta_{mono} + (L - 1)\eta_{off}}{L} \quad (18)$$

where L is the total number of layers of the multilayer film. The initial QY, $\eta_{0,multi}$, and saturated QY, $\eta_{s,multi}$, of the QD multilayer are respectively represented as

$$\eta_{0,multi} = \frac{\eta_{0,mono} + (L - 1)\eta_{off}}{L} \quad (19a)$$

$$\eta_{s,multi} = \frac{\eta_{s,mono} + (L - 1)\eta_{off}}{L} \quad (19b)$$

3. Experimental Methods

3.1. Fabrication of Mono- and Multilayer QD Films. Tri-*n*-octylphosphine oxide (TOPO)-capped CdSe/ZnS core/shell QDs were synthesized by a known colloidal chemistry method as previously reported.[19] Briefly, TOPO-capped CdSe cores were synthesized using CdO and a Se-tributylphosphine complex as precursors according to the method described in ref 21. The average diameter of the cores was estimated to be 3.1 nm from the exciton absorption peak wavelength (550 nm).[22] ZnS shells were grown on CdSe cores using $Zn[S_2CNEt_2]_2$ as a single-molecule precursor according to the method described in ref 23. Because the thickness of the ZnS shell was calculated to be about two monolayers, the average diameter of core/shell QDs, d, was estimated to be 4.2 nm using the bulk lattice parameter of ZnS.[24] The estimated QD size agrees with the average diameter of CdSe/ZnS QDs determined from TEM micrographs (ca. 4.5 nm). The CdSe/ZnS QDs were dispersed in chloroform (99+%, Wako Pure Chemicals) to QD concentrations of 0.1 and 1.0 wt %. Then each dispersion was spin coated onto precleaned cover glasses (25 mmφ, Fisher Scientific) at 3000 rpm for 60 s. The obtained QD films were preserved under vacuum in the dark.

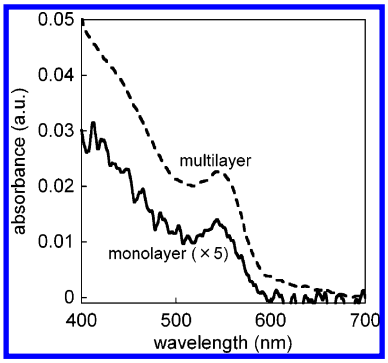

Figure 2. Absorption spectra of the QD monolayer (solid line) and the QD multilayer (dashed line).

TABLE 1: Excitation Wavelengths, Absorption Cross Sections, Excitation Powers, Excitation Intensities, and Excitation Rates

λ (nm)	σ (cm^2)	laser power (μW)	I (kW/cm^2)	k_{exc} (s^{-1})
405	1.92×10^{-15}	4.31−39.6	3.92−36.0	1.53×10^7−1.41×10^8
458	1.29×10^{-15}	0.90−26.0	0.64−18.5	1.91×10^6−5.50×10^7
488	1.02×10^{-15}	0.78−165	0.49−103	1.23×10^6−2.59×10^8
514	7.92×10^{-16}	0.76−306	0.43−173	8.76×10^5−3.54×10^8

3.2. AFM Observation and UV−Vis Spectroscopy. The thickness of the QD film was measured by using AFM (SPA 300HV, Seiko Instruments). A flat homogeneous QD layer was observed when the 0.1 wt % dispersion was used. The glass substrate was partially observed in defects of the film. Because the height difference between the surface of the QD film and that of the substrate was 4−5 nm ($\cong d$), the film obtained from the 0.1 wt % dispersion is considered to be a monolayer of QDs.

The absorption spectra of the QD films as shown in Figure 2 were obtained by using a UV−vis spectrometer (U-4100, Hitachi). By carrying out baseline compensation using the absorption spectrum of the thin TOPO film on the glass substrate, we obtained the absorbance of a QD monolayer, A_{mono}. The absorption cross section of QDs is given by $\sigma = 2.3A_{mono}/(Nd)$, where N (cm^{-3}) represents the number of QDs per unit volume. Assuming hexagonal close-packing of QDs in the monolayer, N is calculated to be 1.6×10^{19} cm^{-3}. As a result, σ values for different excitation wavelengths (405, 458, 488, and 514 nm) were estimated and are shown in Table 1. The order of the obtained σ agreed with the value reported in the literature.[1,25] In the case of the multilayer, the absorbance A_{multi} is obtained in the same way as for the monolayer. The absorption cross section can be written as $\sigma = 2.3A_{multi}/(NLd)$. From the values of σ for the monolayer below a wavelength of 570 nm, $L = 8$−10 is obtained, and we use $L = 9$ in the following discussion.

3.3. Fluorescence Measurements. Fluorescence spectra were measured using a Jasco FP-6500 fluorescence spectrophotometer. The peak wavelength and the full width at half-maximum of the fluorescence spectrum of the QD/toluene dispersion were 571 and 34 nm, respectively. The time evolution of the area intensity of the fluorescence spectrum (530−600 nm) was

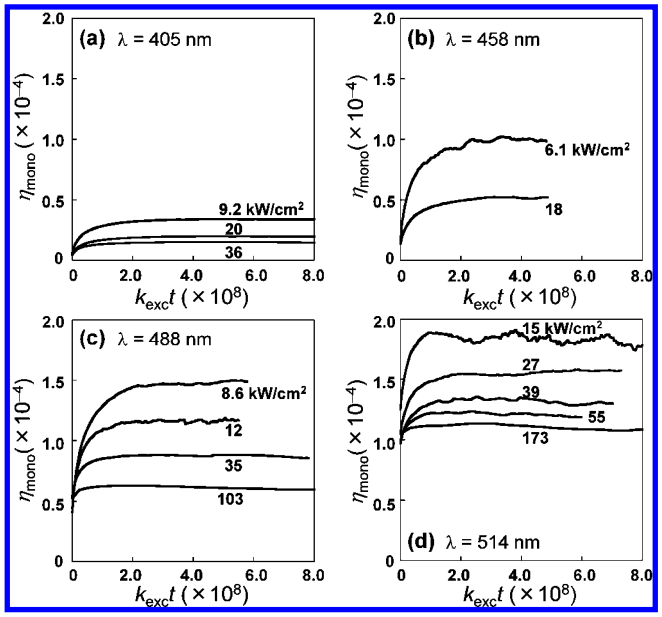

Figure 3. Evolution of the QY of the monolayer η_{mono} obtained by continuous irradiation at various excitation intensities for (a) 405, (b) 458, (c) 488, and (d) 514 nm excitation wavelengths. The numbers by the lines show the excitation intensities (kW/cm^2).

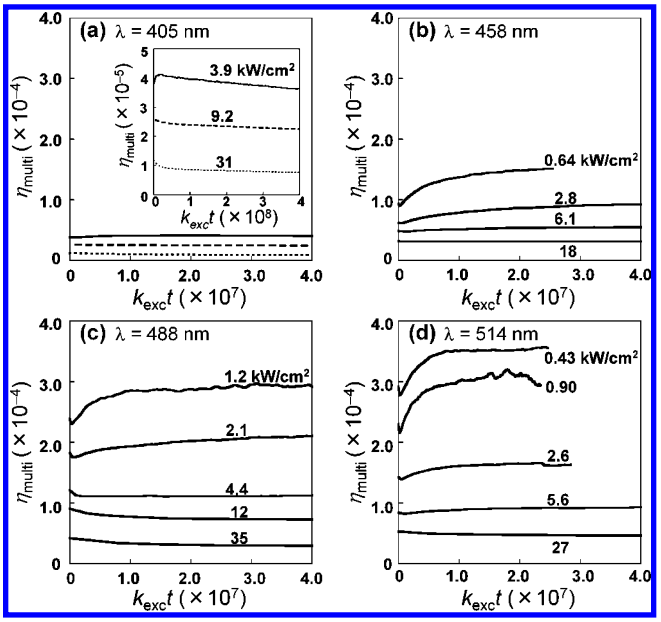

Figure 4. Evolution of the QY of the multilayer η_{multi} obtained by continuous irradiation at various excitation intensities for (a) 405, (b) 458, (c) 488, and (d) 514 nm excitation wavelengths. In part a, solid, dashed, and dotted lines represent the data for 3.9, 9.2, and 31 kW/cm^2 excitation intensities, respectively. In parts b−d, the numbers by the lines represent the excitation intensities (kW/cm^2). The inset in part a shows the evolution curves plotted for a longer time showing the fluorescence intensity decay.

measured by confocal laser scanning microscopy (CLSM; TCS-SP2, Leica) as described in the previous paper.[20] The QD film was covered by a handmade polystyrene cell, and the cell was purged with dry N_2 gas for more than 2 h before the time-course measurement to replace the air completely. There was a continuous flow of dry N_2 gas during the measurement to keep the relative humidity below 0.3% (at 25 ± 2 °C). A 7.4 μm^2 area was continuously scanned by a 405 nm semiconductor laser and a CW Ar laser (458, 488, and 514 nm). The laser power at the sample position was tuned by a neutral density filter, and it was measured by an OPHIR PD300-SH power meter. Because the laser beam was focused by an oil-immersion lens (NA = 1.32), the diameter of the beam spot D (cm) was estimated to be $D \cong (1.22\lambda/\mathrm{NA}) \times 10^7$, where λ (nm) is the wavelength of the laser beam. The excitation intensity per unit area I was calculated from the measured power and the estimated spot area ($\pi D^2/4$).

The range of I with respect to the four excitation wavelengths used in the experiments and the calculated rate constant of excitation, k_{exc} (s^{-1}), are shown in Table 1. From the voltage-gain correlation properties of the photomultiplier (R6358, Hamamatsu), the average brightness of the fluorescence image was recalculated from the supplied voltage of the photomultiplier, and then the relative fluorescence area intensity was obtained. The actual irradiation time was estimated to be 0.1 s/scan because the laser beam of spot size D took 1.63 s for one scan of a 7.4 μm^2 area, as previously reported.[20]

4. Results and Discussion

Figure 3 shows η_{mono} values obtained by irradiation at various intensities of the four different excitation wavelengths plotted as a function of $k_{exc}t$, which represents the integration value of the number of photons absorbed by the QD film. The initial QY, $\eta_{0,mono}$, is constant at all excitation intensities as seen in Figure 3. Subsequent irradiation increases η_{mono}, and the rate of increase of η_{mono} depends on the excitation intensity, I. The saturated QY, $\eta_{s,mono}$, increased with decreasing I at any λ, and the dependence on I is much more prominent for a smaller λ. In addition, the total number of photons required for saturating η_{mono} was almost constant, regardless of I and λ. The noisy curves for η_{mono} observed with 458 and 514 nm excitation (Figure 3b and d) are due to the fluctuation of the sample stage of the CLSM. Next, η_{multi} was plotted as a function of $k_{exc}t$ as shown in Figure 4. The initial value of QY, $\eta_{0,multi}$, strongly depends on I, unlike the situation for the monolayer film. The rate of increase of η_{multi} increases with decreasing I, as is the case for the monolayer film. However, the rate of increase of η_{multi} is substantially smaller than that of η_{mono}. (The maximum $\eta_{s,mono}/\eta_{0,mono}$ is 6.2, whereas $\eta_{s,multi}/\eta_{0,multi}$ is 1.6 at most). When the multilayer film is irradiated at a strong intensity, fluorescence intensity decay is observed as shown in the inset of Figure 4a. A comparison of the results for mono- and multilayer films suggests that the glass substrate plays an important role, in view of the facts that $\eta_{0,mono}$ is I-invariant and that the rate of increase of η_{mono} is much larger than that of η_{multi}. In the previous study, the rate of fluorescence intensity increase was found to increase with increasing proximity of the CdSe/ZnS QDs in a submonolayer covered with a SiO_x protective layer.[19] The results suggest that the electrostatic potential produced by an electron ejected from a QD suppresses the further ionization of adjacent QDs and the total emission efficiency of the QD film increases.

To consider the excitation intensity dependence of $\eta_{0,mono}$ and $\eta_{s,mono}$ in comparison to that of the model, $\eta_{0,mono}$ and $\eta_{s,mono}$ at each λ are plotted against k_{exc} as shown in Figure 5a. $\eta_{0,mono}$ was almost constant, whereas $\eta_{s,mono}$ increased with decreasing k_{exc}. First, the k_{exc} dependence of $\eta_{s,mono}$ is explained by eq 12. The rate constant of radiative recombination k_r is fixed at 10^7 s^{-1}.[5] Although $\eta_{s,\,mono}$ increases with increasing α according to eq 12 in our model, α is fixed at $\alpha = 5$ on the basis of the previous report.[18] The value of C is estimated to range from 6×10^{-4} to 1×10^{-3} because the large $\eta_{s,mono}$ in the case of $\lambda =$ 514 nm cannot be reproduced by the model when $C < 6 \times 10^{-4}$ and because the k_{exc} dependence of $\eta_{s,mono}$ in cases when $\lambda =$ 405 and 458 nm cannot be reproduced when $C > 1 \times 10^{-3}$. Thus, C is fixed at 8×10^{-4} in all of the calculations. On

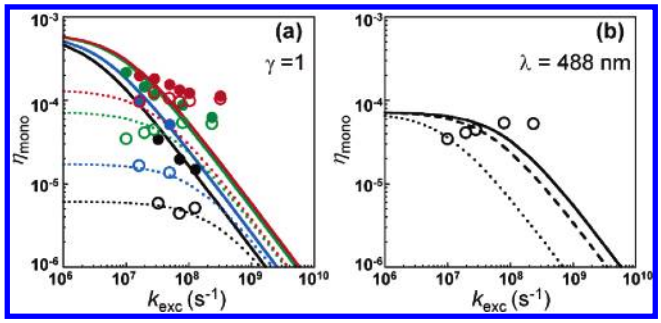

Figure 5. (a) Initial and saturated QY of the monolayer ($\eta_{0,mono}$ and $\eta_{s,mono}$) vs the rate constant of excitation k_{exc}. Open and filled circles represent the experimental data for $\eta_{0,mono}$ and $\eta_{s,mono}$, respectively. Dotted and solid lines represent the theoretical curves for $\eta_{0,mono}$ and $\eta_{s,mono}$ calculated from eqs 11 and 12, respectively. Black, blue, green, and red colors correspond to 405, 458, 488, and 514 nm excitation wavelengths, respectively. (b) Results for the fitting of $\eta_{0,mono}$ in the case with 488 nm excitation. Solid, dashed, and dotted lines represent $\eta_{0,mono}$ calculated with $\gamma(= k^0_{sn}/k_{sr}) = 0.1$, 1.0, and 10, respectively. The open circles correspond to the experimental data as in part a.

TABLE 2: Excitation Wavelengths, Rate Ratios between $|E\rangle \rightarrow |T_c\rangle$ and $|T_c\rangle \rightarrow |E\rangle$ Transitions, Initial Values of the Rates of the $|E\rangle \rightarrow |T_{sn}\rangle$ Transition, and Tunneling Distances

λ (nm)	$\beta (= k_c/k_{cr})$	k^0_{sn} (s^{-1})	l (nm)
405	2.8	1.3×10^9	0.95
458	1.5	4.5×10^8	0.93
488	0.25	1.0×10^8	0.99
514	<0.1	5.0×10^7	1.03

the basis of the above-mentioned conditions, eq 12 was fitted to the experimental data of $\eta_{s,mono}$ with β as an adjusting parameter. The calculated results are shown by solid lines in Figure 5a, and the values of β obtained by the fitting are shown in Table 2. As shown in Table 2, the value of β increases with decreasing λ. Note that if $\beta < 0.1$ the denominator of eq 12 can be approximated as $k_{exc} + k_r$ and the curve of $\eta_{s,mono}$ barely changes. The results indicate that the rate of ionization into trap sites in the capping agents increases with decreasing λ. Next, eq 11 was fitted to the experimental data of $\eta_{0,mono}$ with k^0_{sn} and γ as adjusting parameters, using the β values obtained in the previous section (Table 2). The fitting results are shown by dotted lines in Figure 5a. Figure 5b shows the results in the case of $\lambda = 488$ nm, with γ varying from 0.1 to 10 by fixing k^0_{sn} at 1.0×10^8 s^{-1}. As seen in Figure 5b, the constant value of $\eta_{0,mono}$ at a small k_{exc} is determined not by γ but by k^0_{sn}. When γ decreases, the range of k_{exc}, where $\eta_{0,mono}$ is constant, becomes broad, and the calculated result agrees better with the experimental data. However, it is not realistic that the neutralization from trap sites is much faster than the ionization. Therefore, γ is fixed at 1.0 in the model. The value of k^0_{sn} obtained from the fitting increases with decreasing λ as shown in Table 2.

In the case of strong irradiation ($I > 0.1$ kW/cm^2), Auger-assisted tunneling is dominant as an ionization process.[25] If the Auger event occurs prior to the relaxation of the highly excited electron to the conduction band of the QD, then Auger-assisted photoejection takes place via one photon plus a second electron−hole pair with energy $\Delta E_g + h\nu$.[5] Here, ΔE_g is the band gap energy of a CdSe QD. The result that β increases with decreasing λ can be explained by this wavelength-dependent Auger energy. Similarly, the electron ejection to the substrate is thought to be the Auger-assisted tunneling process for which the rate constant can be described as $k^0_{sn} = k^0_{tunneling} \exp(-\sqrt{8m\Delta E/\hbar^2}\, l)$ on the basis of the 1D tunneling model.[5] Here, m (kg), ΔE (eV), and l (nm) denote the electron mass, the tunneling barrier energy, and the tunneling distance, respectively. $k^0_{tunneling}$ is a preexponential factor, and the typical value of $k^0_{tunneling} = 10^{14}$ s^{-1} is used. If Auger-assisted tunneling from $|E\rangle$ takes place, then ΔE can be written as $\Delta E = \Delta E_C - h\nu$. Here, $\Delta E_C = 4.3$ eV is the energy difference between the conduction band of the QD and the vacuum level (i.e., the electron affinity of the QD[26]). From the above considerations, l can be estimated as shown in Table 2. The values of l at each λ were almost in agreement with the thickness of a TOPO layer (~1 nm).[27] Therefore, the λ dependence of β and k^0_{sn} can be interpreted as being due to this wavelength-dependent Auger energy.

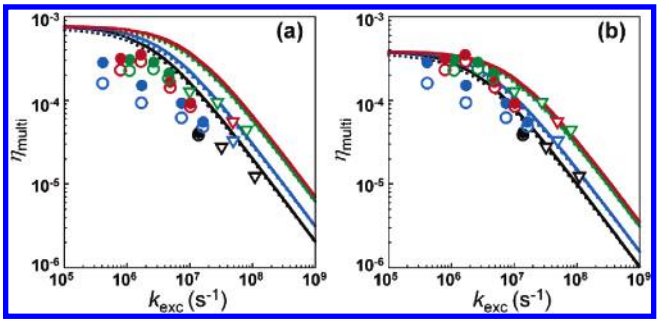

Figure 6. (a) Initial and saturated QY of the multilayer ($\eta_{0,multi}$ and $\eta_{s,multi}$) vs the rate constant of excitation k_{exc}. Open and filled circles represent the experimental data for $\eta_{0,multi}$ and $\eta_{s,multi}$, respectively. Dotted and solid lines represent the theoretical curves for $\eta_{0,multi}$ and $\eta_{s,multi}$ calculated from eqs 19a and 19b, respectively. Black, blue, green, and red colors correspond to 405, 458, 488, and 514 nm excitation wavelengths, respectively. (b) Calculated values of $\eta_{0,multi}$ and $\eta_{s,multi}$ are halved in order to compare them with the experimental data. The same symbols as in part a are used.

The almost constant $\eta_{0,mono}$ at any k_{exc} can be explained by the assumption that the neutralization process of the electron in $|T_{sn}\rangle$ is dominated by the $|T_{sn}\rangle \rightarrow |G\rangle$ transition (section 2). If the electron situated in $|T_{sn}\rangle$ returns to $|E\rangle$, then the steady-state approximation of eq 4 gives $\overline{\phi_g} = (k_r/k_{exc})\overline{\phi_e}$ because $k_{sr}\phi_{sn}$ can be neglected. Then, the steady-state fraction of electrons in $|E\rangle$ is calculated to be $\overline{\phi_e} = (1 - \phi_{sf})/(k_r/k_{exc} + 1 + k_c/k_{cr} + k_{sn}/k_{sr})$, and one obtains

$$\eta_{0,mono} = \frac{Ck_r}{(1 + \beta + \gamma)k_{exc} + k_r} \qquad (20)$$

Comparing eq 20 with eq 11, $\eta_{0,mono}$ depends on k_{exc} more than in eq 11 because of the lack of k^0_{sn} in the denominator. In other words, the plateau of $\eta_{0,mono}$ seen in Figure 5 cannot be explained if we assume a $|T_{sn}\rangle \rightarrow |E\rangle$ transition instead of a $|T_{sn}\rangle \rightarrow |G\rangle$ transition. After continuous irradiation, the ionization to the substrate is suppressed, and the $|E\rangle \rightarrow |T_c\rangle$ transition becomes dominant in the present model. Thus, $\eta_{s,mono}$ depends on k_{exc}.

When $\lambda = 488$ and 514 nm, however, the experimental data deviate from the theoretical curves (Figure 5). The deviation may be due to the uncertainty in k_{exc}. The estimated spot size of the irradiation light, D, is the minimum size calculated from the lens properties. If the irradiation light broadens, then the irradiation intensity I decreases. In addition, σ may include an error of a factor of 2−3. Therefore, it is possible that the actual k_{exc} is much smaller than the estimated k_{exc}. If the experimental data of η_{mono} are plotted using smaller values of k_{exc}, then the fitting improves.

The initial and saturated QYs of the multilayer films ($\eta_{0,multi}$ and $\eta_{s,multi}$) are plotted as a function of k_{exc} in Figure 6a. The

open triangles represent $\eta_{0,multi}$ when $\eta_{s,multi}$ cannot be determined because of the fluorescence intensity decay that does not show saturation within our experimental time scale. In addition, Figure 6a shows the theoretical curves of $\eta_{0,multi}$ and $\eta_{s,multi}$ calculated from eqs 19a and 19b using the values of β shown in Table 2. Note that when $L > 5$, η_{multi} is approximately equal to η_{off}. At any λ, $\eta_{0,multi}$ and $\eta_{s,multi}$ are almost constant when $k_{exc} < 10^6\ s^{-1}$, and they decrease with increasing k_{exc} when $k_{exc} > 10^6\ s^{-1}$. The behavior of η_{multi} qualitatively agrees with the experimental results, although the calculated values are about two times larger than the experimental data. The discrepancy may be due to the reabsorption of fluorescence by other QDs and/or the smaller irradiation intensity of QDs located at the far side of the lens according to the Lambert−Beer law. If we simply shift the theoretical curves downward by using QY values that have been halved, then they agree well with the experimental data, as shown in Figure 6b.

The rate of increase of the calculated η_{multi} is smaller than that determined from the experimental data of η_{multi}. This discrepancy might be due to the assumption that only the QDs in the first layer near the substrate are influenced by the electrostatic blockade effect (eq 18). If the influence of the electrostatic potential produced by electrons situated in $|T_{sf}\rangle$ extends to the upper layers, then the fluorescence of QDs in the upper layers is somewhat enhanced, and $\eta_{s,multi}$ increases. This idea is consistent with the fact that the maximum rate increase of the QY has been observed in a trilayer QD film sandwiched between two insulating layers.[19] Additionally, T_c actually has various energy levels.[4,5] If long-lived trapped electrons were present in the capping agents, then they would contribute to the ionization-suppression effect in the same way as the electrons in $|T_{sf}\rangle$. This could be another reason for the larger rate of increase for η_{multi} in the experiments as opposed to the calculations.

In summary, the simple model can explain the QY of mono- and multilayer films with two adjusting parameters (k_{sn}^0 and β). The agreement between the experimental data and the theoretical curves suggests that the photoelectrification model describes the PFE mechanism reasonably well. Another important characteristic of PFE is its reversibility. Because the slow recovery of the QY that had been observed after the increase by the PFE phenomenon was observed under dark conditions, the change in QY is reversible as in the previous studies.[19,20] The reversibility can be explained if the slow neutralization of the electrons situated in $|T_{sf}\rangle$ is considered in the photoelectrification model. In fact, Cherniavskaya et al. have reported the neutralization of charged CdSe/CdS QDs on the order of ~5 h.[7] In addition, the PFE competes with the fluorescence intensity decay that is observed at the large I in the cases of QD multilayers. The fluorescence intensity decay could be due to the Auger effect. However, the fluorescence intensity decay cannot be expressed by this simple model because the ratio of the ionization rate to the neutralization rate (β) is constant at any I. To understand the PFE mechanism in detail, it is necessary to consider the electron dynamics in a single QD with respect to the variety of energy levels of the trap sites.

5. Conclusions

Photoinduced fluorescence enhancement (PFE) of mono- and multilayer QD films is observed using various irradiation intensities at four different excitation wavelengths. The rate of increase of the emission efficiency of the monolayer film is much larger than that of the multilayer film. The results suggest that the photoejection of electrons to the substrate is the origin of PFE. The simple model assuming the ionization of electrons into trap sites present in the substrate and in the capping agents successfully explains all major features of the PFE behavior observed in our experiments. This agreement between the theoretical curves and the experimental data suggests that the PFE phenomenon is due to the ionization-suppression effect produced by electrons trapped in the substrate and that the intensity and wavelength of excitation light influence the tunneling process of the electron to the substrate.

Acknowledgment. This work was supported by Research Fellowships of the Japan Society for the Promotion of Science (JSPS) for Young Scientists and by Grants-in-Aid for Scientific Research from the Ministry of Education, Culture, Sports, Science and Technology, Japan (MEXT) and from the "Nanotechnology Materials Program - Nanotechnology Particle Project" of the New Energy and Industrial Technology Development Organization (NEDO) based on funds provided by the Ministry of Economy, Trade and Industry, Japan (METI).

References and Notes

(1) Nirmal, M.; Dabbousi, B. O.; Bawendi, M. G.; Macklin, J. J.; Trautman, J. K.; Harris, T. D.; Brus, L. E. *Nature* **1996**, *383*, 802.
(2) Michler, P.; Imamoglu, A.; Mason, M. D.; Carson, P. J.; Strouse, G. F.; Buratto, S. K. *Nature* **2000**, *406*, 968.
(3) Neuhauser, R. G.; Shimizu, K. T.; Woo, W. K.; Empedocles, S. A.; Bawendi, M. G. *Phys. Rev. Lett.* **2000**, *85*, 3301.
(4) Kuno, M.; Fromm, D. P.; Hamann, H. F.; Gallagher, A.; Nesbitt, D. J. *J. Chem. Phys.* **2000**, *112*, 3117.
(5) Kuno, M.; Fromm, D. P.; Johnson, S. T.; Gallagher, A.; Nesbitt, D. J. *Phys. Rev. B* **2003**, *67*.
(6) Krauss, T. D.; Brus, L. E. *Phys. Rev. Lett.* **1999**, *83*, 4840.
(7) Cherniavskaya, O.; Chen, L. W.; Brus, L. *J. Phys. Chem. B* **2004**, *108*, 4946.
(8) Murray, C. B.; Kagan, C. R.; Bawendi, M. G. *Annu. Rev. Mater. Sci.* **2000**, *30*, 545.
(9) Kagan, C. R.; Murray, C. B.; Bawendi, M. G. *Phys. Rev. B* **1996**, *54*, 8633.
(10) Cordero, S. R.; Carson, P. J.; Estabrook, R. A.; Strouse, G. F.; Buratto, S. K. *J. Phys. Chem. B* **2000**, *104*, 12137.
(11) Nazzal, A. Y.; Qu, L. H.; Peng, X. G.; Xiao, M. *Nano Lett.* **2003**, *3*, 819.
(12) Simurda, M.; Nemec, P.; Trojanek, F.; Maly, P. *Thin Solid Films* **2004**, *453−454*, 300.
(13) Myung, N.; Bae, Y.; Bard, A. J. *Nano Lett.* **2003**, *3*, 747.
(14) Hess, B. C.; Okhrimenko, I. G.; Davis, R. C.; Stevens, B. C.; Schulzke, Q. A.; Wright, K. C.; Bass, C. D.; Evans, C. D.; Summers, S. L. *Phys. Rev. Lett.* **2001**, *86*, 3132.
(15) Jones, M.; Nedeljkovic, J.; Ellingson, R. J.; Nozik, A. J.; Rumbles, G. *J. Phys. Chem. B* **2003**, *107*, 11346.
(16) Oda, M.; Shen, M. Y.; Saito, M.; Goto, T. *J. Lumin.* **2000**, *87−9*, 469.
(17) Maenosono, S.; Ozaki, E.; Yoshie, K.; Yamaguchi, Y. *Jpn. J. Appl. Phys., Part 2* **2001**, *40*, L638.
(18) Maenosono, S. *Chem. Phys. Lett.* **2003**, *376*, 666.
(19) Kimura, J.; Uematsu, T.; Maenosono, S.; Yamaguchi, Y. *J. Phys. Chem. B* **2004**, *108*, 13258.
(20) Uematsu, T.; Kimura, J.; Yamaguchi, Y. *Nanotechnology* **2004**, *15*, 822.
(21) Qu, L. H.; Peng, X. G. *J. Am. Chem. Soc.* **2002**, *124*, 2049.
(22) Yu, W. W.; Qu, L. H.; Guo, W. Z.; Peng, X. G. *Chem. Mater.* **2003**, *15*, 2854.
(23) Malik, M. A.; O'Brien, P.; Revaprasadu, N. *Chem. Mater.* **2002**, *14*, 2004.
(24) Dabbousi, B. O.; RodriguezViejo, J.; Mikulec, F. V.; Heine, J. R.; Mattoussi, H.; Ober, R.; Jensen, K. F.; Bawendi, M. G. *J. Phys. Chem. B* **1997**, *101*, 9463.
(25) Lounis, B.; Bechtel, H. A.; Gerion, D.; Alivisatos, P.; Moerner, W. E. *Chem. Phys. Lett.* **2000**, *329*, 399.
(26) Coe, S.; Woo, W. K.; Bawendi, M.; Bulovic, V. *Nature* **2002**, *420*, 800.
(27) Drndic, M.; Jarosz, M. V.; Morgan, N. Y.; Kastner, M. A.; Bawendi, M. G. *J. Appl. Phys.* **2002**, *92*, 7498.